# First principle studies of B and P doped Si nanocrystals

**Ivan Marri[1], Elena Degoli[2], Stefano Ossicini[*,1,2]**

[1] CNR-Istituto di Nanoscienze-S3, via Campi 213 A, I-41125 Modena, Italy
[2] Dipartimento di Scienze e Metodi dell'Ingegneria, Universitá di Modena e Reggio Emilia, Via Amendola 2 Pad. Morselli, I-42122 Reggio Emilia, Italy

Received XXXX, revised XXXX, accepted XXXX
Published online XXXX

**Key words:** Silicon nanocrystals, doping, optoelectronic properties, ab-initio calculations.

[*] Corresponding author: e-mail stefano.ossicini@unimore.it, Phone: +390 522 522211, Fax: +390 522 5222609

The properties of n- and p- doped silicon nanocrystals obtained through ab-initio calculations are reviewed here. The aim is the understanding of the effect of substitutional doping on the structural, electronic and optical properties of freestanding and matrix-embedded Si nanocrystals. The preferential positioning of the dopants and its effect on the structural properties with respect to the undoped case, as a function of the nanocrystals diameter and termination, are identified through total-energy considerations. The localization of the acceptor and donor related levels in the band gap of the Si nanocrystals, together with the impurity activation energy, are discussed as function of the nanocrystals size. The dopant induced differences in the optical properties with respect to the undoped case are presented. Finally we discuss the case of B and P co-doped nanocrystals showing that, if carriers are perfectly compensated, the Si nanocrystals undergo a minor structural distortion around the impurities inducing a significant decrease of the impurities formation energies with respect to the single doped case. Due to co-doping, additional peaks are introduced in the absorption spectra giving rise to a size-dependent red shift of the absorption spectra.

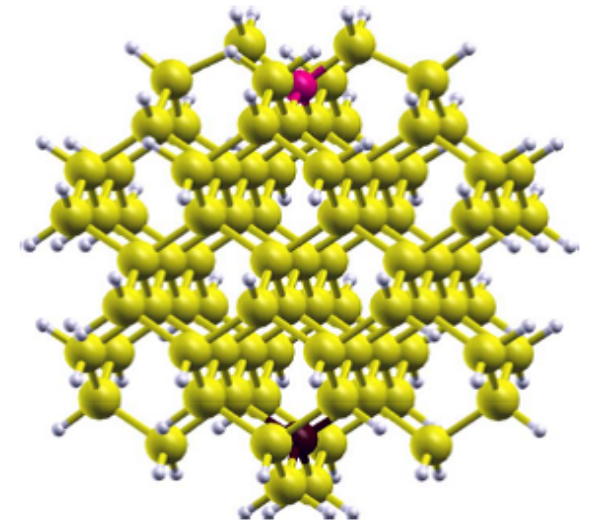

Structure of a co-doped $Si_{85}BPH_{76}$ nanocrystal, diameter 1.56 nm. Yellow (gray) balls represent Si atoms, while the white (light gray) balls are the H atoms used to saturate the surface danglind bonds. B (magenta, dark gray) and P (black) dopants are here located in subsurface positions.



**1 Introduction** The advent of nanoscience and nanotechnologies and the consequent scaling down of Si structures to nanometer sizes have opened new interesting opportunities. In particular the possibility to play with the size, shape and surface termination of silicon nanocrystals (Si-NCs) togheter with their low toxicity and good biocompatibility has prompted their application in microeletronics [1,2], photonics [3,4], non-linear optics [5,6], photovoltaics [7–12], thermoelectrics [13,14] and biomedicine [15,16]. Moreover the doping of Si-NCs, as in the case of bulk semiconductor devices, can be used to alter in a controllable way the electronic, optical and transport proper-

ties of the nanomaterials. Thus one expect that intentional doping with n- and p-type impurities will play a critical role for the design and realization of novel devices based on Si-NCs. Nevertheless several studies have revealed that doping in Si-NCs is quite different from their bulk counterparts [17–19], for example the ionization of the impurities at room temperature may be strongly quenched with respect to the bulk and a shallow impurity level in bulk may become a deep level at the nanoscale. Moreover in the case of nanocrystals there are several possible impurity locations, i. e. within the nanocrystals, at their surface-interface, or in the surrounding matrix, and it is difficult from the experimental point of view to obtain information about the exact dopant location. Our aim here is to review the results of ab-initio calculations regarding the structural, electronic and optical properties of n- and p- doped freestanding and matrix-isolated Si-NCs. Particular attention will given to the discussion regarding the tendency of the dopant atoms to move from the core of the Si-NCs and segregate towards the surface and/or the interface as function of the NCs size [20–26]. Beside the effect of the impurities on the electronic and optical properties of the Si-NCs will be discussed. Indeed results concerning co-doping, i.e. the contemporary presence of group III and group V impurities will be adressed.

**2 Methods** All the structural and optoelectronic properties have been obtained by full ab-initio calculations in the framework of the density functional theory (DFT) using pseudopotentials in the local density aproximation (LDA) [27–29]. When necessary spin-polarized calculations have been performed. It is well known that LDA severly understimates bulk semiconductor energy gap. This inadequacy can be resolved through the inclusions of many-body effects considering the self-energy corrections and the excitonic effects [30]. Nevertheless the results obtained through LDA are interesting for several reasons: i) the inclusion of many-body effects are very computationally demanded and thus limited to very small nanocrystals [31], ii) an almost complete compensation of self-energy and excitonic effect [32–34] has been observed in silicon based nanostructures, thus rendering the LDA based optoelectronic outcomes significative, iii) very often one is interested in trends and trends will remain similar on going from independent-particle approximation to the many-particle corrections. All the considered structures are modeled by using the supercell method by means of cells whose diameters are large enough to make negligible the interaction between the replicas. Ionic relaxation without any symmetry constraint and energy minimization are performed for all the considered systems in order to calculate the full relaxed structures. As p-type dopant we consider B atom and as n-type dopant P atom, owing the fact that doping of Si-NCs with boron and phosphorus has been investigated in detail, throughout the paper we consider substitutional impurities since several experimental studies point towards this type of impurity incorporation. [10, 17–19, 35–37]

**3 Freestanding Si-NCs** For freestanding nanocrystals we consider Si-NCs whose dangling bonds at the surface are passivated with H atoms, which excludes the possible effects of surface dangling bond states and surface reconstructions. Concerning the shape of the Si-NCs, one can consider both spherical-like and faceted Si-NCs. The spherical-like Si-NCs are obtained by cutting Si atoms outside a sphere from Si bulk, whereas the faceted Si-NCs result from a shell-by-shell construction procedure, in which one starts from a central atom and adds shells of atoms successively. We consider nanocrystals whose diameter ranges up to about 3 nm. In H-terminated Si-NCs the dopant atom could be either inside or on the surface, thus the considered dopant locations were all the possible substitutional sites, starting from the center of the Si-NC and moving toward the surface the impurity atom to the other substitutional sites in the entire Si-NC.

**3.1 Formation energies** Starting from a $Si_nH_m$-NC the formation energy for a neutral X impurity can be defined as the energy needed to insert the X atom with chemical potential $\mu_X$ within the NC after removing a Si atom, transferred to the chemical reservoir, assumed to be bulk Si

$$E_f = E(Si_{n1}XH_m - E(Si_nH_m) + \mu_{Si} - \mu_X \quad (1)$$

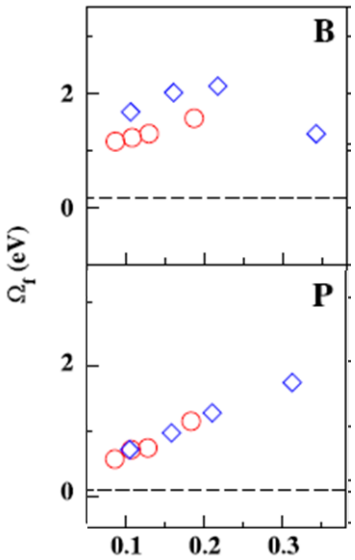


**Figure 1** Impurity formation energies of B and P (located at the center of the Si-NCs) versus the reciprocal radii (in $Å^{-1}$) of the doped Si-NCs (a larger reciprocal radius corresponds to a smaller Si-NC). The energy values are given for faceted (diamonds) and spherical-like (circles) doped Si-NCs. The dashed lines indicate the impurity formation energies in Si bulk.

where E is the total energy of the system, $\mu_{Si}$ is the total energy per atom of bulk Si, and $\mu_X$ is the total energy per atom of the impurity. The formation energies calculated from Eq. 1 are reported in Fig. 1 for B and P impurity located at the center of the Si-NCs.

The formation energy of B and P decreases as the Si-NC size increase, thus showing that larger Si-NC can more easily sustain the B- or P-doping and shows an almost linear dependence on the reciprocal radius of the Si-NC. A comparison between faceted and spherical-like Si-NCs shows that the incorporation of the impurity cost more energy if the Si-NC has facets in the case of B, whereas is nearly shape-independent for P. Clearly for B- and P-doping the impurity formation energies of the Si-NCs are always higher than in Si bulk. These results are related to the deformation of the Si-NC caused by the impurity. The smaller the Si-NC, the larger is the deformation [31]. Moreover since B impurity leads to a simmetry lowering ($C_{3v}$ vs. $T_d$) [21] the impurity formation energies for B are higher. Similar results have been obtained by other authors, confirming that the effect of size is much more evident for B-doping that for P-doping [20,24,38–43]. The size dependence of the calculated formation energy is in qualitative agreement with the observed suppression of the photoluminescence (PL) in doped Si-NCs [44], even if this quenching can be related to impurity-induced defect states in the Si-NCs band gap [45].

It is interesting to see how the formation energy changes as a function of the impurity position within the Si-NC [20,21,38,46,47]. This is an important point because the optical and electrical activity of the dopant atoms depends from their positions. Figure 2 shows the formation energy for the B neutral impurity in a $Si_{146}BH_{100}$-NC (diameter 1.86 nm) [21]. The impurity is moved from the Si-NC center toward the surface along two paths. The results show that the B atom tend to migrate toward the subsurface position. This is explained by considering that such positions are the only ones that allow a significant atomic relaxation around the impurity. Thus, as the B atom is moved toward the surface the formation energy decreases, making the subsurface positions more stable. It is interesting to note that in the case of P impurity it has been showed that these behavior depends on the Si-NC diameter, in fact P atoms prefer to stay at the subsurface positions for Si-NCs with diameter less than 2 nm, whereas for larger nanocrystals the Si-NC center is the energetically most favorable position [46,47].

It should be noted that the impurity formation energies can be influenced by several factors: the presence of vacancy [48], the presence of H deficient Si-NCs surfaces [49], an impurity location directly at the Si-NC surface [50], the substitution of H atoms at the Si-NC surface with a OH group [51,52] showing that, indeed, also small (diameter less than 2 nm) Si-NCs can effectively incorporate B and P impurity atoms.

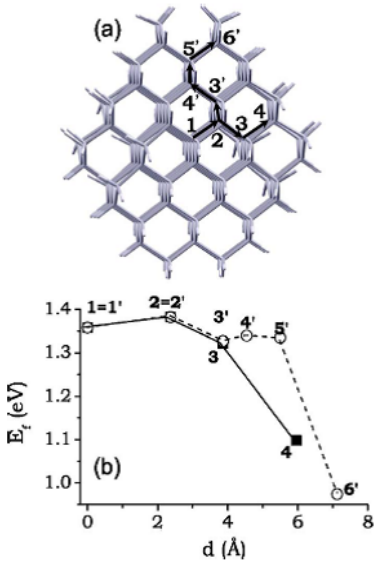


**Figure 2** The B impurity is moved along two different paths toward the Si-NC surface. (b) Formation energies for B neutral impurities as function of the impurity position within the Si-NC.

Regarding the experimental outcomes, freestanding Si-NCs have been synthesized mainly by plasma synthesis [10,18,17,19,35,36] and colloidal chemistry [53,54] showing that were possible to obtain high quality with extremely low defect content Si-NCs with diameter below 3 nm. Moreover also doped Si-NCs have been succesfully sinthesized. However, as pointed out above, it is difficult from the experimental point of view to obtain information about the exact dopant location, nevertheless different techniques have been employed in order to obtain information about the position of the impurity atoms. Electron paramagnetic resonance (EPR) has been used to demonstrate that P impurities are incorporated in substitutional sites [55], a conclusion reached also by electrically detected magnetic resonance (EDMR) [56]. Regarding boron impurity it has been found that the incorporation of B in he Si-NCs is much less efficient with respect to the case of P [57]. This is in agreement with the theoretical results showed in Fig. 1 [58].

However from the experimental outcomes regarding as-grown doped Si-NCs sequentially oxidized and HF etched [57] it seems that, in contrast with the theoretical results for H-terminated Si-NCs, B prefer to stay in the Si-NC core whereas P prefer to stay at the Si-NC surface. Nevertheless it is worthwhile to note that for H-covered Si-NCs with some H deficiency, it has been theoretically shown that P prefer to be located at the Si-NC surface and B in the core [49] in agreement with the experiments and that the experimental results depends on the Si-NCs synthesis procedures. For example Sugimoto et al.[59] have demonstrated that, depending on the etching time, one

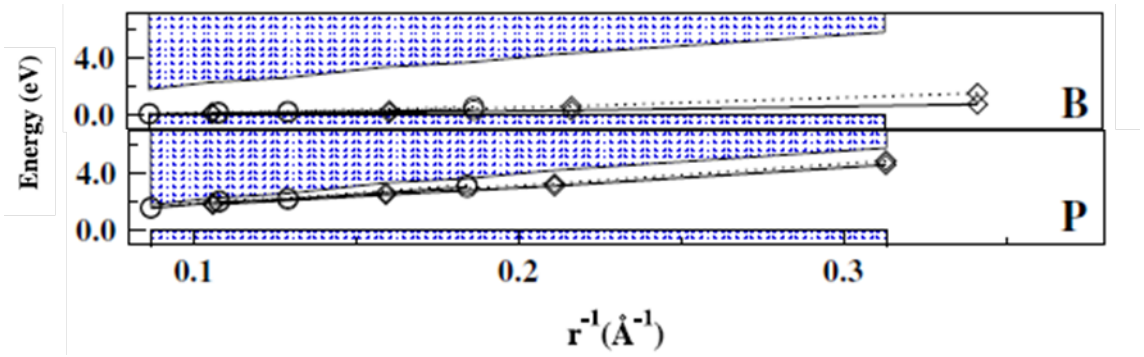


**Figure 3** Energetic position of the DFT calculated impurity levels versus the reciprocal radii of the spherical-like (circles) and faceted (diamonds) Si-NCs. The solid and dotted lines correspond to the spin-up and spin-down impurity levels. The dashed regions represent the occupied and unoccupied elecronic bands of the undoped Si-NCs

can obtain Si-NCs which consists of intrinsic cores and heavily B-doped shells. Indeed, as underlined by Arduca and Perego [18], whereas the theoretical results concerns the thermodynamic stability of the impurity atoms in the Si-NCs, in the experiments is not possible to separate the equilibrium properties from the kinetic effects, which play an important role with respect to doping.

Finally a systematic study of the plasmonic properties of Si-NCs doped with boron and phosphorus through localized surface plasmon resonance demonstrated that the dominant doping mechanism for P is substitutional doping, whereas for B is surface doping [60].

**3.2 Electronic and optical properties** The simple incorporation of B or P impurities in the Si-NCs does not ensure the generation of free majority charge carriers by ionization of the dopant atom at room temperature. The activation of the impurities is related to their binding energy (BE). In bulk semiconductor the BE of the acceptor is defined as the energy difference between the defect level and the valence band maximum (VBM) of the system, whereas the BE of the donor is given by the energy difference between the conduction band minimum (CBM) and the defect level.

In Si-NCs, as consequence of quantum confined effects, size reduction results in a enlargment of the band gap, consequently after doping the relative position of the defect energy level with respect to HOMO and LUMO levels strongly depends on the NC size [46,58]. Moreover, differently form the bulk, the extra hole or electron tends to remain localized near the impurity[20,31]. In order to quantify the position of the impurity-related levels and perform an energy alignment for the electronic levels of the undoped and doped-Si NCs, an energy reference analogous to the VBM in Si bulk and the HOMO in undoped Si-NCs should be determined. In practice, the energy reference of the doped Si-NC does not necessarily coincide with the one of the undoped Si NC. However, the average electrostatic potential at the vacuum region is constant for both doped and undoped Si NCs. We used the difference of the absolute values of the potentials at the vacuum region to perform the energy alignment of the two systems [58, 61].

In figure 3 the position of the impurity levels in the energy-gap region as well as the HOMO-LUMO gap of the undoped Si-NCs shows nearly a linear dependence versus the reciprocal radii of the NCs. The B or P impurity is located at the center of the Si-NCs. A decrease of the Si-NC size, i.e. an increase of quantum confinement, leads to deep impurity levels in the doped Si-NCs. The fact that the positions of the impurity levels vary with size of the Si-NC is important, since other properties of Si-NCs such as the computed [20] and the measured hyperfine splitting [62] are found to have the same dependence on the size. The incorporation of B and P impurities leads to an odd number of electrons, thus the impurity level with the lower energy (spin up or spin down) is occupied and the level with higher energy is not occupied. As shown in figure 3 the increasing

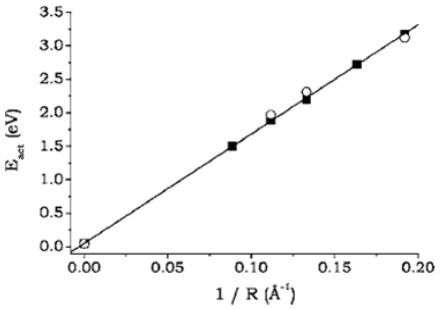


**Figure 4** Impurity activation energy, as a function of the inverse NC radius. Both B- (filled squares) and P-doped (open circles) Si-NC are considered. The zero inverse radius corresponds to bulk Si. The solid line is a linear fit of the data for the B-doped Si-NC. The impurity is located at the Si-NC center.

of quantum confinement, i.e. a reduction of the NC size, results in larger energy differences between the spin-up and spin-down impurity-related levels. The values of the splitting are greater for the B impurity than for P, moreover all these values are always above the corresponding values in Si bulk.

In order to define better the impurity binding energy at the nanoscale one can use the impurity activation energy $E_{act}$ [20,21,63,64] defined a

$$E_{act}(B) = I_u - A_d \quad (2)$$

$$E_{act}(P) = I_d - A_u \quad (3)$$

where I and A give the Si-NC ionization energy and electron affinity, respectively, while the subscripts u and d refer to the pure (undoped) and doped system, respectively. Calculated activation energes for B- and P-doped Si-NCs, with dopants located at the center of the Si-NC, as a function of the Si-NC size [21] are shown in Fig. 4.

The figure show how the activation energy scale almost linearly with the inverse Si-NC radius showing that the main contribution to this energy is due to the almost unscreened Coulomb interaction and to the very localized nature of the impurity states. Similar results have been obtained by other authors [20]. The dopant activation energy depends not only on the Si-NC size, but also on the position of the dopants atom in the Si-NC. On going from the Si-NC center to the Si-NC surface, $E_{act}$ shows variation up to 0.2 eV [20,21,24,65]. All these results show that in Si-NCs the impurity activation energy is quite larger with respect to their Si bulk value (0.045 eV for both B and P), thus impurity ionization in Si-NCs is strongly quenched with respect to the bulk, in agreement with the experiments [55,66,67].

The calculated optical properties are clearly linked to the output of energy level diagrams [58,61,65,68–71]. Figure 5 shows the optical properties (imaginary part of the dielectric function [61]) for B and P doped Si-NCs, whose diameters go from 1.26 to 2.30 nm. Regarding boron we see that the lowest transition energy of the neutral B-impurity tends to zero, as the size of the doped Si-NC increases, because the energy difference between the HOMO and the LUMO of the minority-spin states tends to decrease as the number of electronic states increases. Moreover, the oscillator strength of this transition tends to decrease for large doped Si-NCs. The values of the lowest transition energies of the Si-NCs doped with the ionized B-impurity approach the lowest transition energy of the undoped Si-NCs. For the largest B-doped Si-NC the absorption spectrum looks practically the same as for the undoped Si-NC. This shows that changes in the optical spectra of B-doped Si-NCs should be caused by neutral impurities. Concerning P-doped Si-NCs the impurity-related peaks in the absorption are more or less so intense as in the case of the Si-NCs doped with B and the values of the lowest transition energies of the Si-NCs doped with an ionized P are larger than the lowest transition energy of the Si-NCs doped with a neutral P

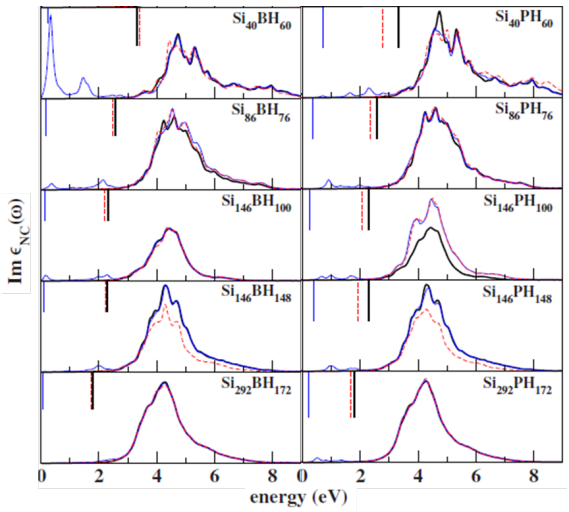


**Figure 5** Optical absorption spectra and energetic position of the lowest optical transition (vertical lines from the top) for the undoped Si-NCs (thick solid lines) and of Si-NCs doped with B and P impurities in their neutral (thin solid line) and ionized (dashed line) charged state.

impurity and slightly red-shifted with respect the ones of undoped Si-NCs. For large Si-NCs the role of P doping is predicted to be more important with respect to of B doping since the B-related peaks practically vanish for the largest Si-NC, in contrast to the P-related peaks. Interestingly high doping levels of P in large Si-NCs have been found to cause efficent absortion of infrared light [72].

**4 Matrix embedded Si-NCs** Matrix-embedded Si-NCs offer advantages in terms of stability and it has been demonstrated that Si-NCs can be easily synthesized within a dielectric matrix using ion implantation [73], plasma enhanced chemical vapor deposition (PECVD) [74] or sputtering [75]. Due to low-cost manufacturability and the possible development of CMOS compatible devices the vast majority of the investigation has been devoted to Si-NCs embedded in a $SiO_2$ host matrix.

Contrary to the case of doping in freestanding Si-NCs there are very few ab-initio theoretical investigations regarding doped Si-NCs embedded in a host matrix. The reason is related to the complicated models needed to simulate these systems, in particular regarding the huge number of atoms involved in the calculations. To overcome this problem Carvalho et al. [76,77] model the embedded Si-NC considering a Si crystalline core of 1.5 nm diameter, surrounded by a $SiO_2$ spherical shell of about 2 nm outer diameter. Their results for the impurity formation energies show that the doping behavior for Si-NCs covered by a $SiO_2$ shell differs from that of the corresponding H-terminated Si-NCs and that the behavior of P is different from that of B. For P doping the impurity prefer to stay in

the Si-NC and not in the silica shell, whereas the formation energy of B impurity is nearly independent on the impurity location, with average formation energies only slightly lower at the interface. Similar results have been obtained by Ni et al. [78,79] studying a 1.4 nm diameter Si-NC covered by 0.25-nm-thick $SiO_2$ shell, whose dangling bonds are saturated by H atoms. They found that B atoms prefer to stay immediately below the $Si/SiO_2$ interface, whereas P atoms are preferentially located in the Si-NC core. Ab-initio calculations for doped Si-NCs clearly embedded in a $SiO_2$ matrix were performed by Guerra et al. [52,80]. The $SiO_2$-embedded Si-NCs have been generated starting from a large $SiO_2$ matrix and removing all the O atoms inside a sphere whose radius determines the Si-NC size. After the ionic relaxation, the $Si/SiO_2$ interface forms stressed bonds, while far from the interface the bulk atomic densities are recovered [33]. Dopant impurity are introduced in a substitutional Si-site located in the Si-NC center, at the $Si/SiO_2$ interface, or in the $SiO_2$ matrix far from the Si-NC. In Fig. 6 the total energy comparison for a $Si_{35}$-NC (diameter about 1 nm) embedded in $SiO_2$, single-doped with a group-V (N or P) or a group-III (Al or B) atom placed at different substitutional sites is showed. In the figure the minimum of each curve identifies the energetically favored site of the corresponding dopant. The data clearly indicate that for n-type doping (P and N) the impurity tends to settle in the Si-NC core, while for p-type doping (Al and B) the interfacial sites are favored.

Experimentally the dopant location for matrix embedded Si-NCs has been studied using three-dimensionally atomic probe tomography (APT) and proximity histogram analysis. Using APT it has been demonstrated that P impurities are efficiently introduced in the core of the Si-NCs, whereas B dopants are located at the $Si\text{-}NC/SiO_2$ interface [81,82]. Also proximity histogram analysis show that P atoms are segregated toward the core of the Si-NC and B atoms at the Si-NC interface [83]. All results in agreement with the theoretical outcomes Furthermore, is clear that in all the considered cases (see Fig. 6) the doping of the $SiO_2$ region is unlikely to occur, especially for n-type doping. In particular, P doping requires a very high formation energy to move the dopant atom from the Si-NC core to the silica, in agreement with the observation that for Si-NCs embedded in a $SiO_2$ matrix, the matrix provides a strong barrier to P diffusion inducing P segregation in the Si rich region [84]. Instead, still consistently with experimental results [85], the diffusion of B toward $SiO_2$ results significantly easier.

**5 Co-doping** Photoluminescence (PL) experiments on doped Si-NCs show that the PL intensity is quenched by the introduction of the impurities [86,87]. It has, hovewer, been shown that this quenching can be avoided when the Si-NCs are simultaneously doped and compensated with B and P impurities. The co-doped Si-NCs exhibit PL energies red-shifted with respect to those of the corresponding

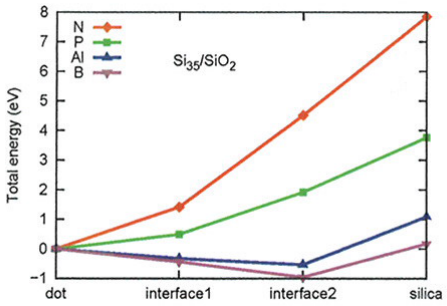


**Figure 6** Total energy of the $Si_{35}$-NC embedded in the $SiO_2$ host matrix and doped with N, P, Al, or B, substitutional of a Si atom in the Si-NC center (core), at the interface bonded to one or two O atoms (interface1, interface 2), or in the $SiO_2$ matrix far from the Si-NC (silica). For a better comprehensibility each line has been shifted so that the structure with the dopant in the Si-NC center has zero energy.

undoped Si-NCs, moreover these energies can range from the visible to below the bandgap energy of the bulk Si [44,88–91]. Thus we will report here the outcomes of a systematic study of the structural, electronic and optical proerties of B and P simultaneously doped Si-NCs using ab-initio DFT calculations [22,31,38–40,52,61,92–98] Starting from the hydrogenated Si-NCs we have co-doped the Si NCs by locating the B and P impurities in all the possible substitutional positions allowing full relaxation with respect to all the atomic positions. Here we will present, in particular, the results relative to the $Si_{85}BPH_{76}$-NC whose relaxed structure is presented in the abstract for the case in wich the impurities are located in substitutional subsurface sites on opposite sides of the Si-NC. In Fig. 7 we report the calculated impurity formation energies (see Eq.

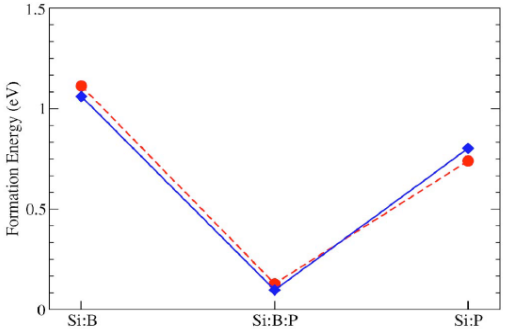


**Figure 7** Impurities formation energies for single-doped and co-doped Si-NCs. In the co-doped Si-NCs, the impurities are located in subsurface substitutional positions on opposite sides of the Si-NC (see next figure). Blue diamonds are related to $Si_{87}H_{76}$-NC (diameter 1.5 nm) and red circles to $Si_{147}H_{100}$-NC (diameter 1.8 nm). The lines are guide for the eyes.

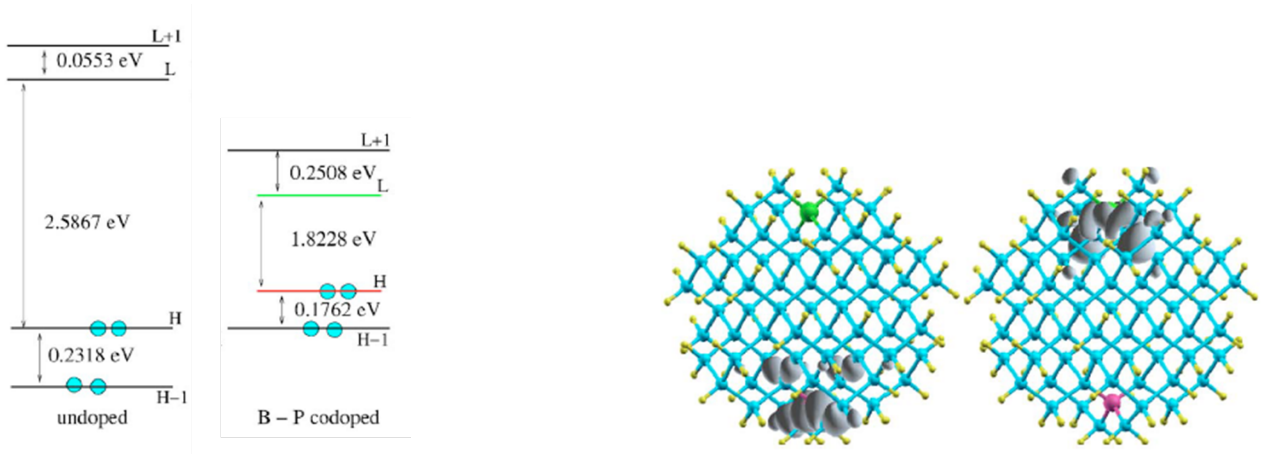


**Figure 8** Left figure : Calculated energy levels at $\Gamma$ for undoped $Si_{87}H_{76}$-NC and co-doped $Si_{85}BPH_{76}$-NC. The alignment has been performed by locating at the same the fully occupied levels with the same type of localization. Right figure: HOMO (left) and LUMO (right) square modulus contour plots calculated for the $Si_{85}BPH_{76}$-NC. Light blue balls represent Si atoms, while the yellow balls are the H atoms used to saturate the surface danglind bonds. B (violet) and P (green) dopants are here located in subsurface positions on opposite sides of the Si-NC.

1) for the $Si_{85}H_{76}$-NC and $Si_{147}H_{100}$-NC. In the figure, we compare the formation energy required to have B or P single-doped Si-NCs with that calculated for the case of B and P co-doped Si-NCs. From Fig. 7 it is clear that simultaneous B and P doping strongly reduces (by about 1 eV) the formation energy with respect to both B or P single doped cases and that this reduction is similar for Si-NCs of different size. While B or P single doping is very costly, B and P co-doping is much easier and there is almost no dependence on the Si-NC size [22]. It is interesting to note that the formation energy of the co-doped Si-NCs depends on the distance between the two impurities. A reduction of the distance between the two impurities results in a reduction of the formation energy. In particular the minimum of the formation energy is obtained when the impurities are located at the nearest neighbors locations at the surface of the Si-NCs. In these cases the formation energy assumes negative values. It is interesting to note that Nomoto et al. [83] have observed that co-doping is an effective means of promoting segregation and stability of the B and P impurities in the Si-NC regions. The fact that Si-NCs can be more easily simultaneously co-doped than single-doped is due to the fact that in the co-doped Si-NCs the differences among the four impurity-Si bond lengths are always smaller with respect to the single-doped case. Thus, if carriers in the Si-NCs are perfectly compensated by simultaneous n- and p-type impurity doping, an almost $T_d$ configuration is recovered in which the four impurity-Si bonds are practically the same [31,52,61].

The electronic properties of B- and P- co-doped Si-NCs are qualitatively and quantitatively different from those of the undoped case and of either B- or P- single-doped Si-NCs. The presence of both a n- and a p-impurity leads to a HOMO level that contains two electrons and to a HOMO-LUMO gap that is strongly lowered with respect to that of the corresponding undoped nanocrystals. The energy levels for the undoped $Si_{87}H_{76}$-NC and co-doped $Si_{85}BPH_{76}$-NC, calculated at the $\Gamma$ point in the optimized geometries, are shown in the left figure of Fig. 8, where only the levels corresponding to the HOMO, LUMO, HOMO-1 and LUMO+1 states are depicted. The calculated square modulus contour plots related to HOMO and LUMO states (see right figure of Fig. 8) show their localization within the Si-NC, in particular the HOMO state is localized on the B impurity while the LUMO is localized on the P one. The presence of these donor and acceptor states lowers the energy gap from 2.59 eV, for the undoped Si-NC, to 1.82 eV, for the co-doped one. For larger Si-NCs and for different impurity locations [31,61,96] it is possible through co-doping also to tune the gap from visible range to below the bulk Si value, in agreement wth the experimental observations [44,88–91].

Recently we have considered a freestanding oxidized Si-NC, the $Si_{87}(OH)_{76}$, co-doped with P and B atoms located at their energetically favored sites: P atom at the Si-NC center and B atom at the Si-NC surface [52]. To investigate the effect of the distance and of the interaction between the dopants we have considered additional nanostructures in which the P atom progressively approaches the B atom (see left figure in Fig. 9). We have numbered the position of the P atom from 5 (Si-NC center) to 1 (Si-NC inner surface). From the analysis of the total energy, reported in the right figure of Fig. 9, it is clear that while in the single-doped Si-NC the P atom stabilize at the Si-NC center, in the co-doped case the formation of a strong P-B bond (position 1) is clearly energetically favored. In alternative, the P-B bond can be formed at the Si-NC center, fulfilling the energetics of the P dopant in the single doped

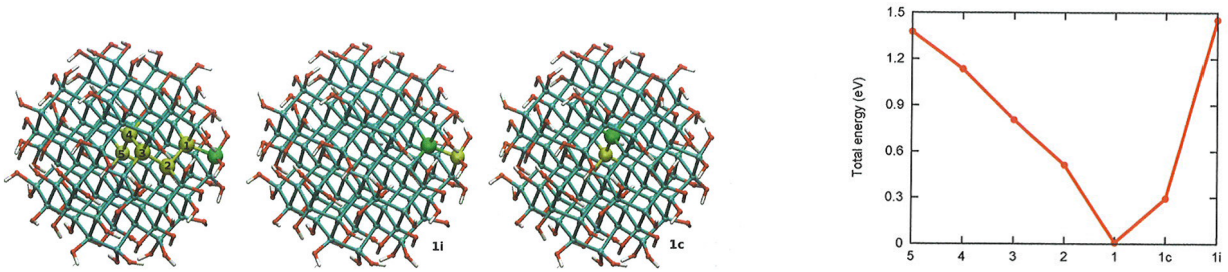


**Figure 9** Left figure: $Si_{85}BP(OH)76$-NC doped (left panel) with B impurity at the surface and P impurity at one of the sites from the center (5) to the nearest neighbor of B (1), doped (central panel) with P placed at the surface and B in the inner nearby (1i); doped (right panel) with P at the Si-NC center and B in the outer nearby (1c). Cyan, red, white, green and yellow balls represent Si, O, H, B, and P atoms, respectively. Right figure: Total energy of the co-doped $Si_{85}BP(OH)76$-NC as function of the dopants position represents in the left figure.

case while forcing the B atom in the NC core. Such configuration, named 1c, results more energetically favored than the 5, 4, 3, and 2 ones, confirming the idea that the formation of the P-B bond prevails with respect to other parameters (see right figure in Fig. 9). wer, the P-B pair at the interface (position 1) remains more stable than that at the Si-NC center (position 1c). Due to the polar nature of the P-B bond, the above condition implies the formation of a static electric dipole radially directed and preferentially located at the Si-NC surface, pointing toward the Si-NC center. Similar results have been obtained by Ni et al. [79]. The high stability of the dipole direction is evidenced by considering a configuration in which the co-dopants are switched, B-P pair, named 1i (see Fig. 9). Quite interestingly, such configuration produces a total energy higher than all the other cases. The formation of stable dipoles at the Si-NCs surfaces radially directed inward the Si-NCs can provide an explanation of the production of stable colloidal co-doped Si-NCs without surface functionalization processes [90, 99–101]

**Acknowledgements** An acknowledgement may be placed at the end of the article.

## References

[1] S. Ossicini, L. Pavesi, and F. Priolo, Springer Tracts in Modern Physics **194**, 1–282 (2003).
[2] D. V. Talapin, J. S. Lee, M. V. Kovalenko, and E. V. Shevchenko, Chem. Rev. **110**, 389–458 (2010).
[3] N. Daldosso and L. Pavesi, Laser & Photon. Rev. **3**, 508–534 (2009).
[4] L. Kriachtchev, S. Ossicini, F. Iacona, and F. Gourbilleau, Int. J. Photoen., 872576 (2012).
[5] Z. Bisadi, M. Mancinelli, S. Manna, S. Tondini, M. Bernard, A. Samusenko, M. Ghulinyan, G. Fontana, P. Bettotti, F. Ramiro-Manzano, G. Pucker, and L. Pavesi, Phys. Status Solidi A **212**, 2659–2671 (2015).
[6] S. V. Makarov, M. I. Petrov, U. Zywietz, V. A. Milichko, D. A. Zuev, N. Lopanitsyna, A. Kuksin, I. Mukhin, G. Zograf, E. Ubyivovk, D. Smirnova, S. Starikov, B. N. Chichkov, and Y. S. Kivshar, Nanolett., 2017 (2017).
[7] F. Priolo, F. Gregorkiewicz, M. Galli, and T. F. Krauss, Nature Nanotechnol. **1**, 19–32 (2014).
[8] M. A. Green, Prog. Photovolt: Res. Appl. **9**, 123–135 (2001).
[9] A. J. Nozik, Nano Lett. **10**, 2735 (2010).
[10] L. Mangolini, J. Vac. Sci. Technol. B **31**, 020801 (2013).
[11] P. Löper, M. Canino, J. López-Vidrier, M. Schnabel, F. Schindler, F. Heinz, A. Witzky, M. Bellettato, M. Allegrezza, D. Hiller, A. Hartel, S. Gutsch, S. Hérnandez, R. Guerra, S. Ossicini, B. Garrido, S. Janz, and M. Zacharias, Phys: Status Solidi A **210**, 669–675 (2013).
[12] C. Summonte, M. Allegrezza, M. Bellettato, F. Liscio, M. Canino, A. Desalvo, J. López-Vidrier, S. Hernández, L. Lopéz-Conesa, S. Estradé, F. Peiró, B. Garrido, P. Löper, M. Schnabel, S. Janz, R. Guerra, and S. Ossicini, Solar Energy Materials & Solar Cells **128**, 138–149 (2014).
[13] M. S. Dresselhaus, C. Gang, Y. T. Ming, Y. Ronggui, L. Hohyun, W. Dezhi, R. Zhifeng, J. P. Fleurial, and P. G, Adv. Mater. **19**, 1043–1053 (2007).
[14] T. Claudio, N. Stein, D. G. Stroppa, B. Klobes, M. M. Koz, P. Kudejova, N. Petermann, H. Wiggers, G. Schierning, and R. P. Hermann, Phys. Chem. Chem. Phys. **16**, 25701–25709 (2014).
[15] F. Erogbobo, K. T. Yong, I. Roy, G. X. Xu, P. N. Prasad, and M. T. Swihart, ACS Nano **2**, 873–878 (2008).
[16] B. F. P. McVey, S. Prabakar, J. J. Goodig, and R. D. Tilley, ChemPlusChem **82**, 60–73 (2017).
[17] B. L. Oliva-Chatelain, T. M. Ticich, and A. R. Barron, Nanoscale **8**, 1733–1745 (2016).
[18] E. Arduca and M. Perego, Materials Science in Semiconductor Processing **62**, 156–170 (2017).
[19] U. R. Kortshagen, R. Mohan Snakaran, R. N. Pereira, S. L. Girshick, J. J. Wu, and E. R. Aydil, Chem. Rev. **116**, 11061–11127 (2016).
[20] D. V. Melnikov and J. R. Chelikowsky, Phys. Rev. Lett. **92**, 046802 (2004).

[21] G. Cantele, E. Degoli, E. Luppi, R. Magri, D. Ninno, G. Jadonisi, and S. Ossicini, Phys. Rev. B **72**, 113303 (2005).
[22] S. Ossicini, E. Degoli, F. Iori, E. Luppi, R. Magri, G. Cantele, F. Trani, and D. Ninno, Appl. Phys Lett. **87**, 1–3 (2005).
[23] G. M. Dalpian and J. R. Chelikowsky, Phys. Rev. Lett. **96**, 226802 (2006).
[24] T. L. Chan, M. L. Tiago, E. Kaxiras, and J. R. Chelikowsky, Nano Lett **8**, 596–600 (2008).
[25] D. J. Norris, A. L. Efros, and S. C. Erwin, Science **319**, 1766–1779 (2008).
[26] J. R. Chelikowsky, M. M. G. Alemany, T. L. Chan, and G. M. Dalpian, Rep. Prog. Phys. **74**, 046501 (2011).
[27] G. Kresse and J. Furthmüller, Comput. Mater. Sci. **6**, 15 (1996).
[28] J. M. Soler, E. Artacho, J. D. Gale, A. Garcia, J. Junquera, P. Ordejón, and D. Sánchez-Portal, J. Phys. Cond. Matter **14**, 2745 (2002).
[29] P. Giannozzi, S. Baroni, N. Bonini, M. Calandra, R. Car, C. Cavazzoni, D. Ceresoli, G. L. Chiarotti, M. Cococcioni, I. Dabo, A. D. Corso, S. de Gironcoli, S. Fabris, G. Fratesi, R. Gebauer, U. Gerstmann, C. Gougoussis, A. Kokalj, M. Lazzeri, L. Martin-Samos, N. Marzari, F. Mauri, R. Mazzarello, S. Paolini, A. Pasquarello, L. Paulatto, C. Sbraccia, S. Scandolo, G. Sclauzero, A. P. Seitsonen, A. Smogunov, P. Umari, and R. M. Wentzcovitch, J. Phys.: Condens. Matter **21**(39), 395502 (2009).
[30] G. Onida, L. Reining, and A. Rubio, Rev. Mod. Phys. **74**(2), 601–659 (2002).
[31] F. Iori, E. Degoli, R. Magri, I. Marri, G. Cantele, D. Ninno, F. Trani, O. Pulci, and S. Ossicini, Phys. Rev. B **76**, 085302 (2007).
[32] M. Luppi and S. Ossicini, Phys. Rev. B **71**, 035340 (2005).
[33] R. Guerra, I. Marri, R. Magri, L. Martin-Samos, O. Pulci, E. Degoli, and S. Ossicini, Phys. Rev. B **79**, 155320 (2009).
[34] R. Guerra, I. Marri, R. Magri, L. Martin-Samos, O. Pulci, E. Degoli, and S. Ossicini, Superl. Microstr. **46**, 246–252 (2009).
[35] R. N. Pereira and A. A. J, J. Phys. D: Appl. Phys. **48**, 314005 (2015).
[36] Z. Ni, X. Pi, M. Ali, S. Zhou, T. Nozaki, and D. Yang, J. Phys. D: Appl. Phys. **48**, 314006 (2015).
[37] M. Fujii, in *Silicon Nanocrystals* ed. by L. Pavesi, and R. Turan pp. (Wiley–Vch, Weinheim 2010) pp. 43–68.
[38] S. Ossicini, F. Iori, E. Degoli, E. Luppi, R. Magri, G. Cantele, F. Trani, and D. Ninno, IEEE J. Sel. Top. Quantum El. **12**, 1585–1591 (2006).
[39] S. Ossicini, E. Degoli, F. Iori, O. Pulci, G. Cantele, R. Magri, O. Bisi, F. Trani, and D. Ninno, Surface Sci. **601**, 2724–2729 (2007).
[40] R. Magri, E. Degoli, F. Iori, E. Luppi, O. Pulci, S. Ossicini, G. Cantele, F. Trani, and D. Ninno, J, Comput. Meth. Sci. Eng. **7**, 219–232 (2007).
[41] G. M. Dalpian and J. R. Chelikowsky, Phys. Rev. Lett. **100**, 179703 (2008).
[42] J. Zeng and H. Yu, J. Nanomater., 147169 (2012).
[43] J. Ma and S. H. Wei, Phys. Rev B **87**, 115318 (2013).
[44] M. Fujii, Y. Yamaguchi, Y. Takae, K. Ninomiya, and S. Hayashi, Appl. Phys. Lett. **85**, 1158–1160 (2004).
[45] D. Hiller, J. López-Vidrier, S. Gutsch, M. Zacharias, K. Nomoto, and D. König, Sci. Rep. **7**, 863 (2017).
[46] Q. Xu, J. W. Luo, S. S. Li, J. B. Xia, J. Li, and S. H. Wei, Phys. Rev. B **75**, 235304 (2007).
[47] T. L. Chan, S. B. Zhang, and J. R. Chelikowsky, Appl. Phys. Lett. **98**, 133116 (2011).
[48] J. H. Eom, T. L. Chan, and J. R. Chelikowsky, Solid State Commun. **150**, 130–132 (201).
[49] J. Ma, S. Wei, N. R. Neale, and A. J. Nozik, Appl. Phys. Lett. **98**, 173103 (2011).
[50] X. Pi, J. Nanomater, 912903 (2012).
[51] A. Carvalho, B. Celikkol, J. Coutinho, and P. Briddon, J. Phys. Conf. Ser. **281**, 012027 (2011).
[52] R. Guerra and S. Ossicini, J. Am. Chem. Soc. **36**, 4404–4409 (2014).
[53] J. G. C. Veinot, Chem. Commun. pp. 4160–4168 (2006).
[54] C. M. Hessel, D. Reid, M. G. Panthani, M. R. Rasch, B. W. Goodfellow, J. W. Wei, H. Fujii, V. Akhavan, and B. A. Korgel, Chem Mat. **24**, 393–401 (2012).
[55] A. R. Stegner, R. N. Pereira, K. Klein, R. Lechner, D. R, S. Brandt, M. Stutzmann, and H. Wiggers, Phys. Rev. Lett. **100**, 026803 (2008).
[56] Y. Nakamine, N. Inaba, K. KoderaT ad Uchida., A. R. PereiraR N amd Stegner., M. S. Brandt, M. Stutzmann, and S. Oda, Jpn. J. Appl. Phys. **50**, 2–7 (2011).
[57] X. D. Pi, R. Gresback, R. W. Liptak, S. A. Campbell, and U. Kortshagen, Appl. Phys. Lett. **92**, 123102 (2008).
[58] L. E. Ramos, E. Degoli, G. Cantele, S. Ossicini, D. Ninno, J. Furthmüller, and F. Bechstedt, J. Phys.: Condens. Matter **19**, 466211 (2007).
[59] H. Sugimoto, M. Fujii, M. Fukuda, K. Imakita, and S. Hayashi, J. Appl. Phys. **110**, 063528 (2011).
[60] N. J. Kramer, K. S. Schramke, and U. R. Kortshagen, Nano Letters **15**, 5597–5603 (2015).
[61] L. E. Ramos, E. Degoli, G. Cantele, S. Ossicini, D. Ninno, J. Furthmüller, and F. Bechstedt, Phys. Rev. B **78**, 235310 (2008).
[62] M. Fujii, A. Mimura, S. Hayashi, Y. Yamamoto, and K. Murakami, Phys. Rev. Lett. **89**, 206805 (2002).
[63] Z. Zhou, M. L. Seigerwald, A. R. Friesner, L. Brus, and M. S. Hybertsen, Phys. Rev. B **71**, 245308 (2005).
[64] M. Lannoo, C. Delerue, and G. Allan, Phys. Rev. Lett. **74**, 3415–3418 (1995).
[65] M. G. Mavros, D. A. Micha, and D. S. Kilin, J. Chem. Phys. C **115**, 19527–19532 (2011).
[66] G. Polisski, D. Kovalev, G. Dollinger, T. Sulima, and F. Koch, Physica B **273-274**, 951–954 (1999).
[67] R. Lechner, A. R. Stegner, R. N. Pereira, R. Dietmueller, M. S. Brandt, A. Ebbers, M. Trocha, H. Wiggers, and M. Stutzmann, J. Appl. Phys. **104**, 053701 (2008).
[68] Z. Zhou, A. R. Friesner, and L. Brus, J. Am. Chem. Soc. **125**, 15559–15607 (2003).
[69] X. Pi, Z. Ni, D. Yang, and C. Delerue, J. Appl. Phys. **116**, 194304 (2014).
[70] X. Pi and C. Delerue, Phys. Rev. Lett. **111**, 177402 (2013).
[71] S. Zhou, X. Pi, Z. Ni, Y. Ding, Y. Jiang, C. Jin, and C. Delerue, ACS Nano **9**, 378–386 (2015).

[72] A. Mimura, M. Fujii, S. Hayashi, D. Kovalev, and F. Koch, Phys. Rev. B **62**, 12625–12627 (2000).
[73] R. Elliman, in *Silicon Nanocrystals* ed. by L. Pavesi, and R. Turan pp. (Wiley–Vch, Weinheim 2010) pp. 223–245.
[74] F. Iacona, G. Franzó, A. Irrera, S. Boninelli, and F. Priolo, in *Silicon Nanocrystals* ed. by L. Pavesi, and R. Turan pp. (Wiley–Vch, Weinheim 2010) pp. 247–273.
[75] F. Gourbilleau, C. Ternon, C. Dufour, X. Portier, and R. Rizk, in *Silicon Nanocrystals* ed. by L. Pavesi, and R. Turan pp. (Wiley–Vch, Weinheim 2010) pp. 275–295.
[76] A. Carvalho, S. Öberg, M. Barroso, M. J. Rayson, and P. Briddon, Phys. Status Solidi A **209**, 1847–1850 (2012).
[77] A. Carvalho, S. Öberg, M. Barroso, M. J. Rayson, and P. Briddon, Phys. Status Solidi B **250**, 1799–1803 (2013).
[78] Z. Ni, X. Pi, and D. Yang, Phys. Rev. B **89**, 035312 (2014).
[79] Z. Ni, X. Pi, S. Cottenier, and D. Yang, Phys. Rev. B **95**, 075307 (2017).
[80] N. Garcia-Castello, S. Illera, J. D. Prades, S. Ossicini, A. Cirera, and R. Guerra, Nanoscale **7**, 12564–12571 (2015).
[81] R. Khelifi, D. Mathiot, R. Gupta, D. Muller, M. Roussel, and S. Duguay, Appl. Phys. Lett. **102**, 013116 (2013).
[82] M. Frégnaus, R. Khelifi, D. Muler, and D. Mathiot, J. Appl. Phys. **116**, 143505 (2014).
[83] K. Nomoto, H. Sugimoto, A. Breen, A. V. Ceguerra, T. Kanno, S. P. Ringer, I. Perez, G. Conibeer, and M. Fujii, J. Phys. Chem. C **120**, 17845–17852 (2016).
[84] M. Perego, G. Seguini, and Fanciulli, Surf. Interface Anal. **45**(1), 386–389 (2013).
[85] M. Xie, D. Li, L. Chen, F. Wang, X. Zhu, and D. Yang, Appl. Phys. Lett. **102**, 123108 (2013).
[86] M. Fujii, S. Hayashi, and K. Yamamoto, J. Appl. Phys. **83**, 7953–7957 (1998).
[87] A. Mimura, M. Fujii, S. Hayashi, and Y. Yamamoto, J. Lumin. **87**, 429–431 (1999).
[88] M. Fujii, Y. Yamaguchi, Y. Takase, K. Ninomiya, and S. Hayashy, Appl. Phys. Lett. **87**, 211919 (2005).
[89] M. Fukuda, M. Fujii, and S. Hayasi, J. Lumin. **131**, 1066–1069 (2011).
[90] H. Sugimoto, M. Fujii, K. Imakita, S. Hayashi, and K. Akamatsu, J. Phys. Chem. C **117**, 11850–11857 (2013).
[91] T. Kanno, H. Sugimoto, A. Fucikova, J. Valenta, and M. Fujii, J. Appl. Phys. **12**, 164307 (2016).
[92] F. Iori, E. Degoli, E. Luppi, R. Magri, I. Marri, G. Cantele, F. Trani, and S. Ossicini, J. Lum. **121**, 335–339 (2006).
[93] F. Iori, S. Ossicini, E. Degoli, E. Luppi, R. Poli, R. Magri, G. Cantele, F. Trani, and D. Ninno, Phys: Status Solidi A **204**, 1312–1317 (2007).
[94] S. Ossicini, O. Bisi, E. Degoli, I. Marri, F. Iori, E. Luppi, R. Magri, R. Poli, G. Cantele, D. Ninno, F. Trani, M. Marsili, O. Pulci, V. Olevano, M. Gatti, K. Gaal-Nagy, A. Incze, and G. Onida, J. Nanosci, Nanotech. **8**, 479–492 (2008).
[95] F. Iori, E. Degoli, M. Palummo, and S. Ossicini, Superl. Microstr. **44**, 337–347 (2008).
[96] F. Iori and S. Ossicini, Physica E **41**, 939–946 (2009).
[97] M. Amato, M. Palummo, R. Rurali, and S. Ossicini, J. Appl. Phys. **112**, 114323 (2012).
[98] M. Amato, M. Palumm, R. Rurali, and S. Ossicini, J. Phys. D: Appl. Phys. **47**, 394013 (2014).
[99] H. Sugimoto, M. Fujii, K. Imakita, S. Hayashi, and K. Akamatsu, J. Phys. Chem C **116**, 19769–19774 (2012).
[100] H. Sugimoto, M. Fujii, K. Imakita, S. Hayashi, and K. Akamatsu, J. Phys. Chem. C **117**, 6807–6813 (2013).
[101] H. Sugimoto, M. Fujii, J. Fukuda, K. Imakita, and K. Akamatsu, Nanoscale **6**, 122–126 (2014).